Mon. Not. R. Astron. Soc. **000**, 000–000 (0000) Printed 9 June 2010 (MN LATEX style file v2.2)

Oxygen Recombination in the nebular phase of supernovae 1998bw and 2002ap*

I. Maurer[1,**], P. A. Mazzali[1,2,3]
[1] *Max Planck Institut für Astrophysik, Karl-Schwarzschild-Str.1, 85741 Garching, Germany*
[2] *Scuola Normale Superiore, Piazza dei Cavalieri, 7, 56126 Pisa, Italy*
[3] *National Institute for Astrophysics-OAPd, Vicolo dell'Osservatorio, 5, 35122 Padova, Italy*

**maurer@mpa-garching.mpg.de*

9 June 2010

ABSTRACT

Late-time spectra of stripped-envelope CC-SNe are dominated by strong [O I] $\lambda\lambda$6300,6363 emission, caused by thermal electron excitation of forbidden [O I] transitions. The permitted O I 7774 Å line is also often observed. This line cannot result from thermal electron excitation of the oxygen ground state. In this work tests are performed to verify whether the line can be powered by oxygen recombination alone, using the examples of two of the best studied type Ic SNe, 1998bw and 2002ap.

Temperature-dependent effective recombination coefficients for neutral oxygen are calculated using available atomic data. Missing atomic data are computed in a temperature range typical for SN nebulae. Core ejecta models for SNe 1998bw and 2002ap are obtained from modelling their nebular emission spectra so that oxygen recombination line formation is computed consistently with oxygen forbidden line emission.

While SN 2002ap can be explained well by a one dimensional shell model, this seems not to be possible for SN 1998bw, for which a two dimensional model is found. At very late epochs the formation of the O I 7774 Å line can be explained by recombination radiation for both SNe, but at earlier epochs strong absorption is present which may determine the strength of this line even at $\sim$ 200 days.

Key words:

1 INTRODUCTION

Massive stars ($>$ 8 $M_\odot$) collapse when the nuclear fuel in their central regions is consumed, producing a core-collapse supernova (CC-SN) and forming a black hole or a neutron star. CC-SNe with a H-rich spectrum are classified as Type II (Filippenko 1997). If the star was stripped of at least most of its H envelope prior to the explosion, the SNe are classified according to the degree of stripping as Type IIb (strong He lines, and weak but clear H), Type Ib (strong He lines but no H), and Type Ic (no He or H lines).

Some CC-SNe, called broad-lined SNe (BL-SNe), exhibit very broad absorption lines at early times, caused by the presence of sufficiently massive ejecta expanding at high velocities. These SNe are sometimes called hypernovae, and can be associated with long-duration gamma-ray bursts (GRBs) (see Woosley & Bloom 2006, and references therein).

In GRB scenarios a relativistic outflow launched by a central engine deposits some fraction of its energy into the SN ejecta. Since the energy is probably deposited preferentially along the polar axis, the SN might be strongly asymmetric (e.g., Maeda et al. 2002). The nearest, best-studied GRB-SNe are SN 1998bw / GRB 980425 (Galama et al. 1999), SN 2003dh / GRB 030329 (Matheson 2004), SN 2003lw / GRB 031203 (Malesani et al. 2004), and SN 2006aj / GRB/XRF 060218 (Pian et al. 2006). It is not yet fully established whether the GRBs (or X-ray flashes) accompanying nearby CC-SNe share the same properties of high-redshift GRBs. CC-SNe may also be characterised by asphericities, although a jet does not necessarily form (Blondin et al. 2003; Kotake et al. 2004; Moiseenko et al. 2006; Burrows et al. 2007; Takiwaki et al. 2009).

Asphericities in the inner and outer ejecta are evident in at least some CC-SNe. Two clear indicators are velocity differences of Fe and lighter-element lines (e.g., Mazzali et al. 2001), and polarisation measurements (e.g., Höflich 1991). Indirect indications also emerge from a comparison of the inner and outer ejecta velocities (Maurer et al. 2009).

Independent of their type, SNe become increasingly transparent to optical light with time, as the ejecta thin out. At late times ($>$ 200 days after the explosion), the innermost layers of the SN can be observed. This epoch is called

the nebular phase, because the spectrum turns from being dominated by absorption to an emission spectrum, mostly showing forbidden lines. In this phase the radiated energy of a SN is provided by the decay of radioactive ^{56}Co (which is produced by the earlier decay of ^{56}Ni) into ^{56}Fe. Decaying ^{56}Co emits γ-rays and positrons which are absorbed by the SN ejecta. As the deposition rate of γ-rays and positrons depends on the density and ^{56}Ni distribution, the inner parts of the SN dominate the nebular spectra. Therefore the nebular phase is especially suitable for studying the core of SNe.

Several authors have modelled nebular-phase spectra of SNe to derive quantities such as the ^{56}Ni mass (e.g., Mazzali et al. 2004; Stritzinger et al. 2006; Sauer et al. 2006; Maeda et al. 2007a), ejecta velocities (e.g., Mazzali et al. 2007b; Taubenberger et al. 2009; Maurer et al. 2009), asphericities (e.g., Mazzali et al. 2005; Maeda et al. 2006; Mazzali et al. 2007a, 2008), and elemental abundances (e.g., Maeda et al. 2007a,b).

To infer SN core ejecta velocities and geometry usually the [O I] $\lambda\lambda$ 6300, 6364 doublet is investigated, since this is by far the strongest nebular emission line (SNe of type Ic), especially at very late epochs. These lines are formed by thermal electron excitation of the 2p(^{1}D) state. Higher quantum states (n $\geqslant$ 3) cannot be excited by thermal electrons sufficiently because of the large ratio of excitation energy ($\sim$ 9 eV) and electron temperature ($\sim$ 0.4 eV). Possible excitation mechanisms are absorption, non-thermal electrons and recombination.

Previous studies of central oxygen have focused almost exclusively on the [O I] $\lambda\lambda$6300, 6364 doublet. It is useful to investigate whether extending the analysis to other oxygen lines gives a consistent picture. Therefore it is important to understand the formation of these lines in detail.

In Section 2 temperature-dependent effective recombination rates are obtained for the n = 3 levels of neutral oxygen and some quantities relevant for oxygen recombination and emission-line formation in CC-SN nebulae are estimated. A one dimensional shell model for SN 2002ap is described in Section 3 and a two-dimensional model for SN 1998bw in Section 4 emphasising the role of the O I 7774 Å line. Results are discussed in Section 5.

2 OXYGEN LINES IN THE NEBULAR PHASE OF CC-SNE

In this section temperature-dependent effective recombination rates are obtained for the 3s, 3p and 3d triplet and quintet states of neutral oxygen. These rates are used in our nebular code to calculate oxygen recombination line emission. These levels are responsible for O I 7774, 8446, 9264 and 11287 A line emission (see Figure 1 for illustration). We further investigate the relevant processes for oxygen recombination and absorption line formation in the nebular phase of CC-SNe.

Recombination into the 2p singlet states is not important in the CC-SN nebular phase. About 80 $-$ 90% of the radioactive energy is deposited in thermal electrons, while only 10 $-$ 20% goes into ionisation (see below). Since the 2p singlet states can be efficiently excited by thermal electron collisions, the population of these levels is predominantly determined by this process.

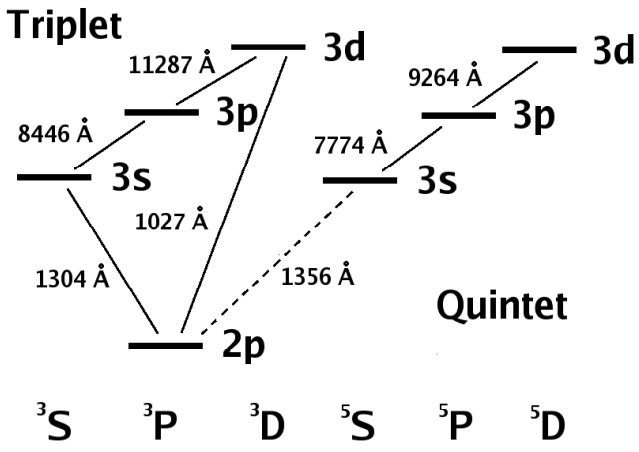

Figure 1. Neutral oxygen levels that are potentially interesting for the nebular phase of CC-SNe. The singlet states (which are responsible for the nebular oxygen forbidden-line emission) and states with n $\geqslant$ 4 are not shown. The 2p, 3p and 3d states can be subdivided into several j sub-states, which are not shown to keep the illustration clear. The wavelengths given represent the mean wavelengths of emission. Lines emitted by the different j sub-states differ slightly from the values given. For example, the line we refer to as O I 7774 Å in this paper consists of three lines at wavelengths 7771.94, 7774.17 and 7775.39 Å. While all transitions indicated by solid lines are permitted with radiative rates of order 10^{7-8} s^{-1}, the 3s(^{5}S) to 2p(^{3}P) transition (spin-forbidden; dashed line) has a radiative rate of order 10^3 s^{-1} only.

2.1 Effective recombination rates for neutral oxygen

Di-electronic recombination is much weaker than radiative recombination [roughly a factor of 5 (Nussbaumer & Storey 1983) at 10000 K and decreasing rapidly with temperature] and is not included when calculating the recombination fractions. At high electron densities collisional transitions between excited states can become important. However, for the electron densities expected in the nebular phase ($n_e < 10^{10}$ cm^{-3}), this effect is weak. At high electron densities ($n_e \sim 10^{10}$ cm^{-3}) and low temperatures ($T \leqslant$ 3000K) collisional recombination can become important (e.g. see Storey & Hummer 1995). However, during the nebular phase only the combinations high density, high temperature (early) and low density, low temperature (late) are important and the contribution of collisional recombination is weak (e.g. $\sim$ 20% at $n_e \sim 10^9$ cm^{-3} and $T \sim$ 5000K).

Therefore we only consider radiative recombination. We are interested in which fraction of recombining electrons reaches a certain atomic level, whether by direct recombination or cascading from higher states. It had been noted by Julienne et al. (1974); Chung et al. (1991) that high quantum levels (n $\sim$ 20) might be important to calculate the recombination cascade. In the literature recombination coefficients and radiative rates are available for neutral oxygen

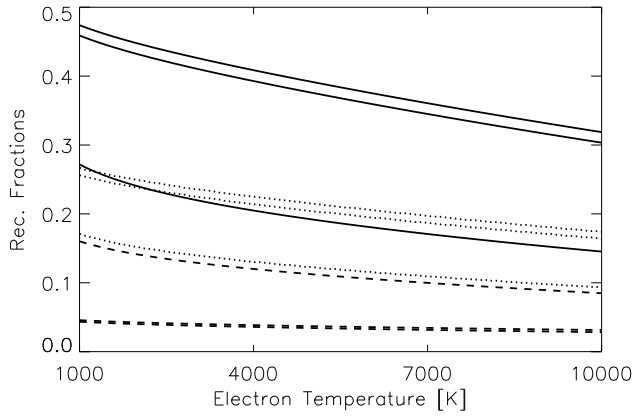

Figure 2. Temperature-dependent normalised effective recombination fractions. The quintet states (3d, 3p, 3s from bottom to top) are shown by solid lines. Triplet states (3p, 3s, 3d from bottom to top; note that 3p and 3s do overlap) for the case of optically thin ground state transitions are shown by dashed lines. Triplet states (3d, 3p, 3s from bottom to top) for the case of optically thick ground state transitions are shown by dotted lines.

up to maximum quantum numbers n $\sim$ 10 (see e.g. TIPTOPbase [1], NIST [2]).

For azimuthal quantum numbers l $\geqslant$ 3 one can use the hydrogenic approximation, however for the s, p and d orbitals this should be avoided (e.g. Chung et al. 1991). Therefore, we obtained radiative recombination coefficients and radiative rates for all s, p and d levels of oxygen up to n = 20 using a quantum defect method (QDM) (Bates & Damgaard 1949; Seaton 1958; Burgess & Seaton 1960).

The potential of the atomic core and the inner electrons approaches the asymptotic form $1/r$ quickly. The wave functions of the excited states can be described by a hydrogen-like solution, with the difference that the quantum energy levels are shifted owing to the unknown structure of the core potential. This shift of energy levels is described by the quantum defect (defined as the difference between the real and 'effective' principal quantum number) and can be measured in experiments or is determined by more sophisticated calculations.

The wave functions calculated by the QDM are described with sufficient accuracy at radii larger than a few (atomic units) and therefore the QDM is reliable as long as the main contribution of the transition integrals comes from sufficiently large radii and there is no strong cancellation in the integrand. Especially for ground state transitions, where contributions from small radii are important, the QDM is therefore not reliable.

To improve the calculation, we numerically integrate the electron wave equation (e.g. Seaton 1958)

$$\Big[\frac{d^2}{dr^2} - \frac{l(l+1)}{r^2} - V(r) + E\Big]P(E,l;r) = 0 \qquad (1)$$

inwards, starting with the solution obtained by the QDM at large radii and using a Thomas-Fermi potential

$$V(r) = \frac{2N}{r}\exp(-Z^{1/3}r) + \frac{2(Z-N)}{r} \qquad (2)$$

where Z is the charge of the nucleus and N the number of core electrons. This integration is not part of the QDM. The Thomas-Fermi potential gives the correct asymptotic behaviour of the atomic potential for $r \to 0$ and $r \to \infty$ (Burke & Robb 1975). The result of this integration is a behaviour of the wave-function for r $\to$ 0 different than predicted by the QDM. For most transitions the contribution from small radii is approximately zero and therefore the calculated rates are not influenced by this correction. For the transitions which are influenced by the inner parts of the wave function we achieve better agreement with oxygen atomic data provided in the literature at low quantum numbers (n < 10).

The difference for ground state radiative transitions relative to NIST recommended data is always less than 50% and the agreement increases considerably with the quantum number of the excited states. For ground state transitions from levels n > 5 the disagreement becomes less than 10%. For transitions between excited states the maximum difference to NIST recommended data is 40% with most transitions agreeing at the 10% level or better. Whenever the disagreement was worse than 10% we replaced our data with the values from the literature. We compared our direct and effective recombination coefficients to Julienne et al. (1974); Chung et al. (1991) and found good agreement (better than 10%), as we did for the effective recombination rates at 1160 K. Our total recombination rate agrees with the value given by Chung et al. (1991) to 1 % at 10000 K. However compared to Aldrovandi & Pequignot (1973) our total recombination rate is $\sim$ 25% too low. It was noted by Julienne et al. (1974) that neglecting the n > 20 levels might cause an underestimate of $\sim$ 20% of the total recombination rate (at temperatures around 1000 K; the effect becomes smaller at higher temperatures). More importantly Aldrovandi & Pequignot (1973) used a hydrogenic approximation for all atomic states, which leads to an overestimate of the recombination rate (Chung et al. 1991). A comparison to a recent calculation from Badnell (2006) shows that our total radiative recombination rates agree to their results within 15% . To handle that deviation, we normalise our result.

We calculate the ratio of the effective recombination rates of the n = 3 levels to the total recombination rate into excited states and find that this ratio varies only weakly with the number of levels included (it changes by $\sim$ 1% (3s), 1% (3p) and 8% (3d) when using a maximum quantum number of n = 20 instead of n = 10) and is not too sensitive to uncertainties in the atomic data (see below), while the total recombination rate is (it increases by 15 - 30% depending on temperature when using a maximum quantum number n = 20 instead of n = 10).

Since fitting formulae for the total and ground state recombination rates are available in the literature, we can obtain the total recombination rate into excited states and normalise our effective recombination rates to the total radiative recombination rate. We call this the normalised effective recombination fraction.

The recombination rates used for this normalisation are

[1] http://cdsweb.u-strasbg.fr/topbase/
[2] http://www.nist.gov/index.html

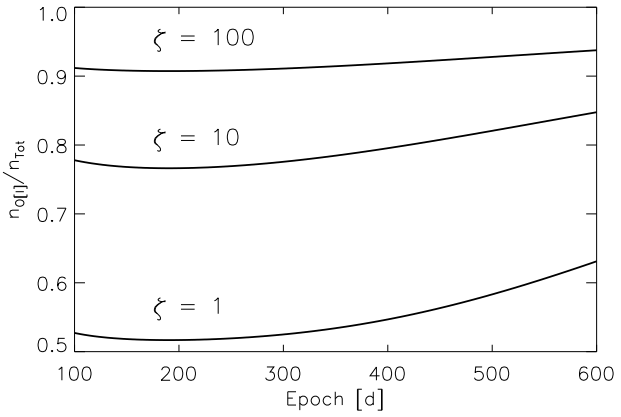

Figure 3. The ratio $n_{\rm O[I]}/n_{\rm Tot}$ for different clumping factors ($\zeta = 1$, 10, 100 from bottom to top) calculated for the test model described in Appendix A. Since clumping increases recombination the fraction of neutral oxygen increases with ζ.

the total recombination rate of Badnell (2006)

$$R_{\rm O[I]} = A\left[\sqrt{\frac{T}{T_0}}\Big(1+\frac{T}{T_0}\Big)^{1-B'}\Big(1+\frac{T}{T_1}\Big)^{1+B'}\right]^{-1} {\rm cm^3 s^{-1}} \quad (3)$$

with $B' = B + C\exp\big(-\frac{T_2}{T}\big)$, $A = 6.622\cdot10^{-11}$, $B = 0.6109$, $C = 0.4093$, $T_0 = 4.136$, $T_1 = 4.214\cdot10^6$ and $T_2 = 8.770\cdot10^4$ and the (direct) ground state recombination rate of Pequignot (1990)

$$\begin{aligned} R_{\rm GS} = {} & (1.174 + 0.2463x + 0.2144x^2 - 0.0621x^3) \\ & \times 10^{-13} T_4^{-0.5} {\rm cm^3 s^{-1}} \end{aligned} \quad (4)$$

with $x = \log(1+T_4)/\log(2)$ and $T_4 = T/10000$ K. These normalised effective recombination fractions are shown in Figure 2 and are listed in Appendix B. To obtain absolute values one has to multiply by the total radiative recombination rate. Since the total recombination rate contains a contribution from direct ground state recombination and since lower levels contain cascading contributions from higher states, these fractions do not add up to one.

Since there are uncertainties in our atomic data we want to quantify their influence. We randomly vary all the radiative rates obtained by the QDM by a value between ± 20% and the recombination rates obtained by the QDM by a value between ± 50% several times. This should be larger than the typical error, at least for excited states. The resulting deviations from the standard values are typically a few percent, often $\ll 5\%$.

2.2 Recombination line formation

With the effective recombination rates shown in Figure 2 it is possible to calculate the strength of all [O I] n = 3 lines due to recombining electrons.

The population of excited oxygen levels by recombination is implemented in the one dimensional (Mazzali et al. 2001, 2007a) and three dimensional version (Maurer et al. 2009) of our nebular code and will be used in Sections 3 and 4 to calculate synthetic recombination lines for SNe 1998bw and 2002ap.

However, to obtain insight into the formation of these lines it is useful to derive some estimates for the recombination line formation. Below, we estimate the strength of the O I 7774 Å line. This is the strongest non-ground state (NGS) recombination line thanks to its high effective recombination rate and transition energy [3p(^{5}P) to 3s(^{5}S)]. Ground state recombination line observations are usually not available since most spectra reach a minimum wavelength of 3000 Å − 4000 Å only.

The ionisation rate can be calculated using the concept of 'work per ion' (e.g. Axelrod 1980), which describes the energy lost to thermal electrons in order to produce one ionisation. The ionisation rate per atom and ion is then given by

$$Y_{\rm O[I]} = \frac{L_{\rm Dep}}{N_{\rm Tot} W_{\rm O[I]}} \quad (5)$$

where $L_{\rm Dep}$ is the total deposited luminosity, $N_{\rm Tot}$ is the total number of atoms and $W_{O[I]}$ is the energy lost to thermal electrons per ionisation and can be estimated by comparing the ionisation cross-section with atomic and plasma loss functions (more details are given in Section 2.5).

During the first several hundred days of a SN, ionisation balance is a valid assumption (Axelrod 1980), therefore

$$Y_{\rm O[I]}(1+\mathcal{R})n_{\rm O[I]} = Y'_{\rm O[I]} n_{\rm O[I]} = R_{\rm O[I]} n_{\rm e} \zeta n_{\rm O[II]} \quad (6)$$

where $\mathcal{R}$ is the recycling fraction (recombination radiation causes further ionisation and $\mathcal{R}$ is expected to have a value between 0.3 and 0.5; Axelrod 1980) and ζ is the clumping factor (explained in more detail below), defined as the inverse of the filling factor (Li & McCray 1992).

Since oxygen is the dominant element in CC-SNe cores [$\sim$ 55 % in SN 2002ap and $\sim$ 75 % in SN 1998bw, as obtained from our modelling in Sections 3 and 4; see also Mazzali et al. (2001, 2007a)] and the degree of ionisation of oxygen is rather high (roughly $10 - 50\%$; Figure 3) it is a reasonable simplification to neglect all elements besides the iron-group elements and oxygen when calculating the ionisation balance and to assume that all electrons are provided by oxygen and by iron, which is assumed to be 100% singly ionised. Therefore

$$Y'_{\rm O[I]} n_{\rm O[I]} \sim R_{\rm O[I]}(n_{\rm O[II]} + n_{\rm Fe})\zeta n_{\rm O[II]} \quad (7)$$

which gives

$$\begin{aligned} \frac{n_{\rm O[I]}}{n_{\rm Tot}} \sim {} & 1 - \frac{n_{\rm Fe}}{n_{\rm Tot}} - \frac{R_{\rm O[I]} n_{\rm Fe}\zeta + Y'_{\rm O[I]}}{2R_{\rm O[I]} n_{\rm Tot}\zeta} \\ & \times \left(-1 + \sqrt{1 + \frac{4Y'_{\rm O[I]} R_{\rm O[I]}(n_{\rm Tot} - n_{\rm Fe})\zeta}{(R_{\rm O[I]} n_{\rm Fe}\zeta + Y'_{\rm O[I]})^2}} \right) \\ \sim {} & 1 - \frac{n_{\rm Fe}}{n_{\rm Tot}} + \frac{R_{\rm O[I]} n_{\rm Fe}\zeta + Y'_{\rm O[I]}}{2R_{\rm O[I]} n_{\rm Tot}\zeta} \\ & - \sqrt{\frac{Y'_{\rm O[I]}(n_{\rm Tot} - n_{\rm Fe})}{R_{\rm O[I]} n_{\rm Tot}^2 \zeta}}\,, \qquad \frac{Y'_{\rm O[I]}(n_{\rm Tot} - n_{\rm Fe})}{R_{\rm O[I]} n_{\rm Tot}^2 \zeta} \gg 1 \\ \sim {} & 1 - \frac{n_{\rm Fe}}{n_{\rm Tot}} \\ & - \frac{Y(n_{\rm Tot} - n_{\rm Fe})}{(R_{\rm O[I]} n_{\rm Fe}\zeta + Y'_{\rm O[I]}) n_{\rm Tot}}\,, \qquad \frac{Y'_{\rm O[I]}(n_{\rm Tot} - n_{\rm Fe})}{R_{\rm O[I]} n_{\rm Tot}^2 \zeta} \ll 1 \end{aligned} \quad (8)$$

In Figure 3 this ratio is computed for a test model described

in Appendix A using clumping factors of 1, 10 and 100. The total luminosity of any recombination line X of oxygen relative to the total deposited luminosity is then given by

$$\begin{aligned}\frac{L_{\rm X}}{L_{\rm Dep}} &= Y'_{\rm O[I]} n_{\rm O[I]} V E_{\rm X} f_{\rm X} L_{\rm Dep}^{-1} \\ &= (1+\mathcal{R})\frac{E_{\rm X} f_{\rm X}}{W_{\rm O[I]}}\Big(\frac{n_{\rm O[I]}}{n_{\rm Tot}}\Big)\end{aligned} \tag{9}$$

where E_X is the energy and f_X is the normalised effective recombination fraction of the line. Usually one can assume $4Y'_{\rm O[I]} R_{\rm O[I]} n_{\rm Tot}\zeta \gg (R_{\rm O[I]} n_{\rm Fe}\zeta + Y'_{\rm O[I]})^2$; see Appendix A. L_{Dep} (e.g. Axelrod 1980) and all other variables (besides the temperature) can be calculated for any ejecta model and Equation 9 can be evaluated directly. The temperature can be determined by balancing heating and cooling taking into account several hundred emission lines (therefore an exact estimate of the temperature is difficult) and varies between 8000 K and 2000 K at the epochs of interest (100 to 600 days). A sufficiently exact estimate can be obtained assuming a constant temperature of $\sim$ 4000 K (see Appendix A).

The luminosity of any oxygen recombination line is directly proportional to the normalised effective recombination fraction $f_{\rm X}$ and the energy of the transition $E_{\rm X}$ [eV]. The recombination line luminosity is influenced only weakly by the clumping factor ζ (which changes the ionisation fraction). The oxygen NGS recombination lines will be weak in general [taking $n_{\rm O[I]}/n_{\rm Tot} \sim 0.5$, $f_{7774} \sim 0.4$, $E_{7774} \sim 1.6$ eV and $W_{\rm O[I]} \sim 75$ eV the strongest NGS oxygen recombination line (7774 Å) carries less than 1.0% of the total luminosity] and we will neglect all other NGS oxygen recombination lines in the rest of this paper. They are calculated by the nebular code, but in the nebular spectra of SNe 1998bw and 2002ap on oxygen recombination lines other than 7774 Å can be identified.

2.3 Excitation of the O I 7774 Å line

We will find in Sections 3 and 4 that the luminosity provided by recombination is not sufficient to explain the observations of the 7774 Å line earlier than $\sim$ 250 days. Therefore, in this section we investigate other excitation mechanisms which might operate simultaneously with recombination.

Ground-state excitation by thermal electrons can clearly be ruled out. All transitions from n $\geqslant$ 3 to the ground state have energies larger than 9 eV, which makes thermal excitation by electrons of temperatures $\sim$ 0.5 eV ineffective.

Non-thermal excitation by the same electrons causing ionisation (which are produced by Compton-scattering of γ-rays emitted by ^{56}Co decay) is also too weak. The ratio of the cross-sections for electron impact excitation and ionisation (at the high electron energies which are of interest here) can be approximated by (e.g. Rozsnyai et al. 1980)

$$\frac{\sigma_{\rm nl\rightarrow n'l'}}{\sigma_{\rm nl}} \sim 1.66\frac{f_{\rm nl\rightarrow n'l'} E_{\rm nl}}{N_{\rm nl} E_{\rm nl\rightarrow n'l'}} \tag{10}$$

where $\rm E_{nl\rightarrow n'l'}$ is the transition energy, $\rm E_{nl}$ the ionisation energy, $N_{\rm nl}$ is the number of electrons in the shell n, l and $\rm f_{nl\rightarrow n'l'}$ the oscillator strength of the transition. We compare hydrogen and helium non-thermal excitation rates obtained by this approximation to values obtained from more sophisticated calculations (Hachinger in prep.), solving an energy-balance equation derived from the Spencer-Fano equation (Xu & McCray 1991; Lucy 1991) and find that the agreement is always better than 30%, which suggests that this approximation is also of acceptable accuracy for oxygen. For allowed ground state transitions of neutral oxygen the oscillator strengths are of the order of 10^{-2} decreasing with increasing quantum number (Bell & Hibbert 1990). The total excitation rate into triplet states is $\sim$ 5% of the ionisation rate only. The excitation rates of quinted states by non-thermal (high-energetic) electrons is even lower, since the excitation cross-sections of spin-forbidden lines strongly decrease with electron energy, as compared to allowed transitions (e.g. Ralchenko et al. 2008).

Therefore, non-thermal excitation is not important compared to recombination for populating excited levels. In addition, if the O I 7774 Å line was excited by non-thermal electrons, one would expect the ratio of the line to the total luminosity to be approximately constant at all epochs, which is clearly not observed (this ratio in fact decreases considerably at late epochs).

Although it is generally assumed that the SN is optically thin during the nebular phase, some lines can still be optically thick (especially ground state transitions). However, as we show here, the optical depth of the 7774 Å transition is still high, even at epochs of $\sim$ 200 days because the 3s(^{5}S) level is populated by recombining electrons.

We estimate the time-dependent optical depth of the 7774 Å line resulting from recombination taking into account the effective recombination rates, resonance scattering of the 3s(^{5}S) to 2p(^{3}P) transition as well as the recycling of ground state recombination radiation.

Based on Equations 7 and 8, the number density of the 3s(^{5}S) state relative to the total density is approximately given by

$$\begin{aligned}\frac{n_{3s(^5S)}}{n_{\rm Tot}} &\sim \frac{f_{3s(^5S)} R_{\rm O[I]}(n_{\rm Fe}+n_{\rm O[II]})\zeta n_{\rm O[II]}}{(A'+C)n_{\rm Tot}} \\ &\sim \frac{f_{3s(^5S)} Y'_{\rm O[I]}\tau}{A}\Big(\frac{n_{\rm O[I]}}{n_{\rm Tot}}\Big)\,, \qquad A \gg A' \gg C \\ &\sim (1+\mathcal{R})\frac{f_{3s(^5S)}\tau_0 L_{\rm Dep}}{AVW_{\rm O[I]}}\Big(\frac{n_{\rm O[I]}}{n_{\rm Tot}}\Big)^2\zeta\end{aligned} \tag{11}$$

defining A' as the reduced (due to self-absorption) radiative rate

$$A' = A\frac{1-\exp(-\tau)}{\tau} \sim \frac{A}{\tau}\,, \qquad \tau \gg 1 \tag{12}$$

from the 3s(^{5}S) to the ground state, where τ is the Sobolev optical depth of this ground state transition

$$\tau \sim \frac{\lambda_{1355}^3 t g_{3s(^5S)} A_{1355} n_{\rm O[I]}\zeta}{8\pi g_{2p(^3P)}} \sim \tau_0\zeta n_{\rm O[I]}\,, \quad n_{\rm O[I]} \gg n_{3s(^5S)} \tag{13}$$

with the ground state transition wavelength $\lambda_{1355} = 1355$ Å, t the epoch in seconds, V the volume in cm^3, A_{1355} the radiative rates from the 3s(^{5}S) to the ground state (note that the ground state is split into three j sub-levels and appropriate weights have to be used; also the radiative rates of these j sub-state transitions differ). The weights of the upper and lower states are $g_{3s(^5S),2p(^3P)}$; $f_{3s(^5S)}$ is the normalised effective recombination fraction into the 3s(^{5}S) state and C

is the de-excitation rate due to thermal electrons which is much smaller than A/τ. The 3s(^{5}S) to 2p(^{3}P) transition is spin-forbidden but dipole-allowed and therefore collisional rates are weaker than radiative rates by several orders in magnitude (van Regemorter 1962) for typical SN nebular densities. For $n_{\rm O}\zeta > 10^9$ cm^{-3} this assumption breaks down since C and τ will increase with density and clumping factor.

Equation 11 can be used to calculate the Sobolev optical depth of the 7774 Å line

$$\tau_{3s(^5S)} \sim \frac{\lambda_{7774}^3 t g_{3p(^5P)} A_{7774} n_{3s(^5S)}[\zeta]}{8\pi g_{3s(^5S)}} \ , \quad n_{3s(^5S)} \gg n_{3p(^5P)} \tag{14}$$

with the transition wavelength $\lambda_{7774} = 7774$ Å, t the epoch in seconds, A_{7774} the radiative rates from the 3p(^{5}P) to the 3s(^{5}S) state (note that the 3p(^{5}P) state is split into three j sub-levels and appropriate weights have to be used) and $g_{3p(^5P),3s(^5S)}$ the weights of the upper and lower states. Again we compare this estimate with numerical results from our nebular code in Appendix A.

At this point it is important review the concept of clumping in more detail. It is assumed that the ejecta are distributed into small "blobs" with size much smaller than the typical scale of the SN, covering the SN volume homogeneously (e.g. Li & McCray 1992). Therefore, although the optical depth is increased locally in the emitting region, the global optical depth of the SN remains constant. This means that, when scattering radiation from remote regions of the SN, the opacity is not influenced directly by clumping. On the other hand, when scattering radiation in the emission region, the optical depth increases proportionally to the clumping factor.

In addition, there is an increase of the ratio $\frac{n_{3s(^5S)}}{n_{\rm Tot}}$ (see Equation 11), which results from the increased self-absorption of ground state transition radiation. Therefore, even when scattering radiation from remote regions, clumping increases the optical depth and so it does influence the 7774 Å resonance scattering of background radiation.

The 3p(^{5}P) state is separated from the 3s(^{5}S) state by ~ 1.6 eV, therefore thermal electron excitation is possible, but the population of the 3s(^{5}S) state by thermal electron excitation is too low. Therefore the state must be populated by recombining electrons.

The thermal electron excitation coefficient from 3s(^{5}S) to 3p(^{5}P) is given by

$$\begin{aligned} C_{3p(^5P)} &\sim 8.6\times10^{-6}\frac{n_{\rm e}\zeta}{T^{1/2}}\frac{\Omega_{7774}}{g_{3s(^5S)}}\exp(-\frac{E_{7774}}{kT}) \\ &\equiv C_0 n_{\rm e}\zeta \end{aligned} \tag{15}$$

where all constants have the same meaning as in Equation 14, E_{7774} is the energy corresponding to 7774 Å and Ω_{7774} = 25.1/40.2 (at 5000/10000 K; Bhatia & Kastner 1995) is the effective collision strength of the O I 7774 Å transition. One can compare the population of the 3p(^{5}P) state due to thermal electron collisional excitation and recombination respectively by calculating their ratio

$$\begin{aligned} \mathcal{R}_{3p(^5P)} &= \frac{C_{3p(^5P)} n_{3s(^5S)}}{Y_{\rm O[I]} n_{\rm O[I]} f_{3p(^5P)}} \\ &= (1+\mathcal{R}) C_0 \frac{f_{3s(^5S)}}{f_{3p(^5P)}}\frac{\tau_0}{A}(n_{\rm Tot}-n_{\rm O[I]})n_{\rm O[I]}\zeta^2 \end{aligned} \tag{16}$$

The ratio of the O I 7774 Å luminosity induced by thermal electron excitation compared to the total deposited luminosity is then given by

$$\begin{aligned} \frac{L_{3p(^5P)}}{L_{Dep}} &\sim (1+\mathcal{R})^2 \frac{C_0 E_{7774} f_{3s(^5S)}\tau_0}{W_{\rm O[I]} A}(1-\frac{n_{\rm O[I]}}{n_{\rm Tot}})n_{\rm O[I]}^2\zeta^2 \\ &\sim 10^{-21} t[\text{days}](1-\frac{n_{\rm O[I]}}{n_{\rm Tot}})n_{\rm O[I]}^2\zeta^2, \quad T = 5000 \text{ K} \end{aligned} \tag{17}$$

This estimate becomes invalid for $n_{\rm O[I]}\zeta > 10^9$ cm^{-3} since Equation 11 had been used for its derivation. Equation 17 is compared to results from our nebular code in Appendix A. Whether collisional excitation of the O I 7774 Å line is negligible depends mainly on the temperature, which decreases with time, on the density of neutral oxygen, which decreases with t^{-3}, and on the clumping factor. Therefore, especially for early epochs (high temperature, high density) and for large clumping factors ($\zeta \gg 1$) the O I 7774 Å line may be excited by thermal excitation of recombining electrons. Around 150 days the core (oxygen) density of CC-SNe is typically of order 10^{7-8} cm^{-3}, which gives $\frac{L_{3p(^5P)}}{L_{Dep}} \sim (10^{-5}$ to $10^{-3})\zeta^2$ assuming a temperature of 5000 K.

From the above considerations it becomes clear that clumping influences the recombination line strength only weakly, but increases the effect of resonance scattering and thermal excitation of the O I 7774 Å transition strongly. For both processes the 3s(^{5}S) population is provided by recombination and not by thermal electron excitation from the ground level.

2.4 Emission versus absorption line shapes

Since the [O I] λλ 6300,6363 doublet has often been used to probe the ejecta velocity and the geometry of CC-SNe cores (see Section 1) it is interesting to study the profile of the [O I] 7774 Å line. If this line were caused by recombination or thermal excitation alone, one would expect that the shapes of the 6300, 6363 and 7774 Å lines should be at least approximately similar.

However, as we have shown above, O I 7774 Å might result from line scattering even at 200 days. At later times the line usually becomes very weak and it is difficult to use it to probe the ejecta geometry. The profile of a scattering dominated line depends on the flux distribution, so one cannot expect that the shape of the 6300, 6363 Å lines and the 7774 Å line will be even approximately similar.

To demonstrate this, we use a multi-dimensional Montecarlo code. A photon background is generated and resonance-scattered in an (asymmetric) oxygen distribution (e.g. taken from a nebular model; the nebular code in its current version cannot simulate scattering processes). We calculate the [O I] λλ 6300,6363 doublet for an asymmetric oxygen model and use the 7774 Å line opacity calculated in the nebular code to compute the absorption of a broad-band

[h]

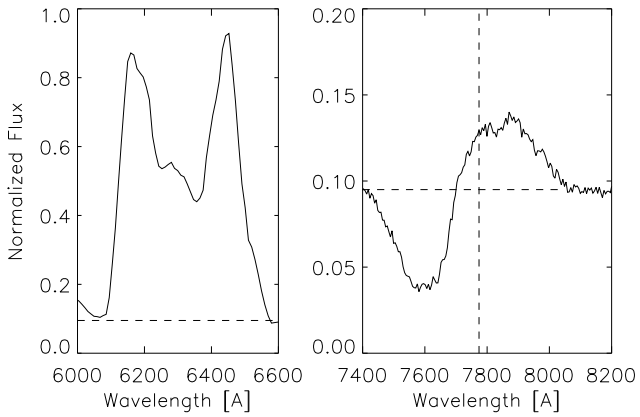

Figure 4. Left side: flux of a synthetic [O I] λλ 6300,6363 doublet for an asymmetric model (double-peaked shape). Right side: the 7774 Å line opacity calculated from this asymmetric model was used to calculate the flux of the absorption line at 7774 Å (dashed vertical line). The flux is normalised to an arbitrary constant. The formation of the absorption line strongly depends on the assumed background (indicated by the dashed horizontal line; it not only depends on the absolute background flux but also on the background rest-frame wavelength which determines the emission site) and therefore the absorption line shown would look different for a different background radiation field. The asymmetry has some influence on the absorption line, but the clear double-peaked shape of the [O I] λλ 6300,6363 doublet is not seen.

background (3000 − 10000 Å) emitted in the inner region of the model SN. The formation of the absorption line is very sensitive to this background and therefore our results (see Figure 4) illustrate just one of many possibilities. As expected, the absorption line has quite a different shape than the emission line.

2.5 Ionisation Rates for the nebular code

To improve the accuracy of the recombination line calculation in our nebular code we updated the treatment of ionisation for all the ions treated. This is necessary, since the formation of recombination lines is much more sensitive to the ionisation rate than the formation of other emission lines, and higher accuracy is needed. In the older version of the nebular code the ionisation rates were calculated using a simple analytical form.

To obtain more accurate ionisation rates we calculate the average 'work per ion' W (see Axelrod 1980), which is the amount of energy lost by a non-thermal electron (with energy $\gg 1$ keV) to cause one ionisation. The ionisation rate is then computed dividing the total deposited luminosity by this energy.

The value of W can be calculated averaging the 'work per ion' $W_{\rm i}^*$ of all individual ions over the total ionisation cross sections. $W_{\rm i}^*$ can be obtained for any ion integrating the ratio of the energy-dependent ionisation cross section $\sigma_{\rm i}$ and the energy loss functions $L_{\rm i}$ (Axelrod 1980)

$$W_{\rm i}^* = \frac{E_{\rm max}}{\int_{E_{\rm min}}^{E_{\rm max}} \frac{\sigma_i(E')}{L_{\rm i}(E')} dE'} \qquad (18)$$

Highly energetic electrons lose most of their energy to ionisation and to the secondary electrons produced in the ionisation, but also by non-thermal excitation. At low energies, losses to the electron plasma become important, however most of the primary energy is lost in atomic collision processes.

Ionisation cross sections and loss functions can be obtained for any ion from the literature at low electron energies (e.g. Lotz 1967, 1970; Lennon et al. 1988). At high electron energies they can be computed by appropriate extrapolations of the low energy values (Axelrod 1980).

The ionisation rate of any ion is then given by

$$Y_{\rm i} = \frac{L_{\rm Dep}\sigma_{\rm i}}{N_{\rm Tot} W < \sigma >} \equiv \frac{L_{\rm Dep}}{N_{\rm Tot} W_{\rm i}} \qquad (19)$$

The ionisation rates mainly affect the recombination lines but also have some influence on all other emission lines. This will be discussed in Section 5.

3 A SHELL MODEL OF SN 2002AP

SN 2002ap is classified as a broad-lined SN of Type Ic. It had an ejected mass of ~ 2.5 M$_\odot$ and a kinetic energy of $\sim 4 \cdot 10^{51}$ ergs (Mazzali et al. 2007a). The distance and reddening to SN 2002ap are only known approximately. To be consistent with previous work we use $\mu = 29.50$ mag and $E(B-V) = 0.09$ mag as done by Mazzali et al. (2002); Yoshii et al. (2003); Mazzali et al. (2007a). It is not clear whether SN 2002ap was a spherical symmetric event or not. Recently, Maurer et al. (2009) have shown that an asymmetry might be observable in all broad-lined CC-SNe, however this point is not clear yet. The spectra of SN 2002ap used in this work are those used by Mazzali et al. (2007a).

Mazzali et al. (2007a) found appropriate one-zone and shell models of the SN 2002ap nebular ejecta. We quickly summarise the main findings for the shell models here. Using a filling factor of 0.1 ($\zeta = 10$) in the ^{56}Ni rich regions, a total ejecta mass of ~ 2.5 M$_\odot$ was found, containing roughly 0.11 M$_\odot$ ^{56}Ni and 1.3 M$_\odot$ of oxygen.

In contrast to this previous work, which aimed at modelling each spectrum individually, here we try to find one single ^{56}Ni/O model which can produce the time evolution of the different spectra at all observed epochs consistently. Special attention is paid to reproducing the exact shape of the [O I] λλ 6300,6363 line profile, which is a tracer of the distribution of oxygen, the most abundant element of the nebula.

Using the same distance modulus and reddening as Mazzali et al. (2007a) and clumping factors of 5 and 25 [we had to use a clumping factor of 1 for the innermost shell of the $\zeta = 25$ model to avoid the formation of sharp high density lines which are not observed; Mazzali et al. (2007a) had used a clumping factor of 10; this will be discussed in Section 5] we obtain models similar to the ones given in Mazzali et al. (2007a) giving reasonable agreement with the observations at all epochs (see Figures 5 and 7). The forbidden oxygen lines are reproduced at all epochs by one and

the same oxygen distribution, which provides evidence for the reliability of this model.

Our ^{56}Ni zone with a total mass of ~ 1.2 M$_\odot$ extends out to 8000 km/s, containing ~ 0.07 M$_\odot$ of ^{56}Ni (in agreement with Mazzali et al. 2002) and ~ 0.7 M$_\odot$ of O. More mass is located at higher velocities, but the nebular modelling becomes inaccurate for the outer regions. The exact values depend on the clumping factor as well as on the ^{56}Ni distribution, which is not known.

The O I 7774 Å line is excited by recombination and thermal electron excitation in our nebular modelling (no line scattering) and is too weak to explain the observations at 129 and 163 days using low clumping factors ($\zeta \sim 5$). The $\zeta = 25$ model can reproduce the observations of the O I 7774 Å line at 129 and 163 days better than the $\zeta = 5$ model. This results from thermal electron scattering of 3s(^{5}S) electrons, which are provided by recombination. In general the $\zeta = 5$ model reproduces the formation of the forbidden lines better than the $\zeta = 25$ model at early epochs, since high density lines, which are not observed, form in the $\zeta = 25$ model.

At days 192 and 229 both models produce too little flux at 7774 Å, which is probably influenced by line scattering at these epochs (the optical depth of the inner shells of the O I 7774 Å line is high for both models at these epochs). The scattering process is not simulated and therefore the synthetic flux is too low.

At later epochs the O I 7774 Å line is consistently reproduced by recombination alone in both models when taking into account the uncertainty due to the background around 7774 Å, which is not reproduced by the nebular code.

The optical depth of the 7774 Å line is shown for all inner shells (five shells between 0 and 5000 km/s) of our $\zeta = 5$ model in Figure 6. It does not fall below one before 210 days, indicating that there can be strong line scattering up to ~ 200 days depending on clumping (for the $\zeta = 25$ model the optical depth is higher and the O I 7774 Å line becomes optically thin later).

For clumping factors below 5 neither line scattering nor thermal excitation was strong enough to allow sufficient formation of the O I 7774 Å line before ~ 200 days.

4 A 2D MODEL OF SN 1998BW

SN 1998bw is classified as a broad-lined SN of type Ic (ejected mass ~ 14 M$_\odot$ and kinetic energy $\sim 6 \cdot 10^{52}$ ergs; Nakamura et al. 2000). We use a distance modulus of $\mu = 32.89$ and an extinction of $A_V = 0.2$ mag as given by Patat et al. (2001). SN 1998bw was accompanied by the low energy, long-duration GRB 980425. Due to this GRB-SN connection there are speculations that SN 1998bw was a highly aspherical event. These speculations are supported by polarisation measurements (Kay et al. 1998; Iwamoto et al. 1998; Patat et al. 2001), which where interpreted as a SN axis ratio of 2:1 (Höflich et al. 1999). Some indication for core ejecta asymmetry had also been found in the nebular spectra of SN 1998bw (Mazzali et al. 2001). The spectra of SN 1998bw used in this work are the same as used by Mazzali et al. (2001) originally presented by Patat et al. (2001).

The nebular phase of SN 1998bw has been well studied by means of nebular modelling (Mazzali et al. 2001;

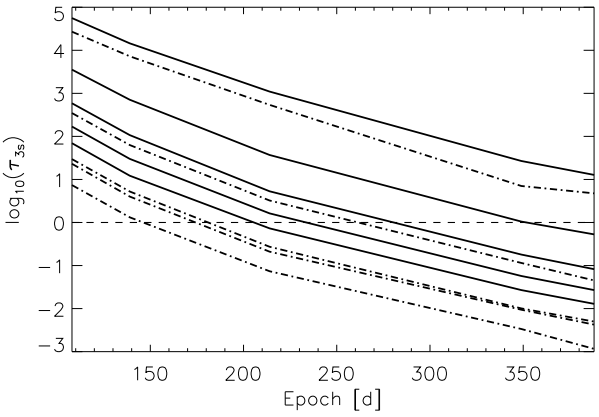

Figure 5. SN 2002ap, models for a clumping factor $\zeta = 5$. Left side: normalised nebular spectra (from top to bottom: 129, 163, 192, 229, 245, 253, 281, 343 and 394 days after explosion) are shown in black with synthetic spectra on top in red. Right side: the region between 7600 Å and 8200 Å is enlarged to enable a comparison of observed (black) and synthetic (red) 7774 Å flux. At epochs of 129 to 229 days, the simulated flux is too low to match the observations. Beginning at 245 days, considering a constant off set caused by background-flux which is not reproduced by the synthetic spectrum, the synthetic 7774 Å line starts to become consistent with the observations.

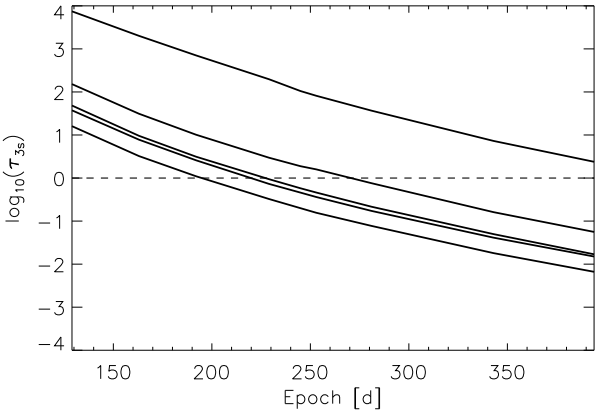

Figure 6. SN 2002ap, models for a clumping factor $\zeta = 5$. The logarithm of the 7774 Å line optical depth in our model for the inner shells (from top to bottom: 0 − 1000 km/s, 1000 − 2000 km/s, 3000 − 4000 km/s, 4000 − 5000 km/s and 2000 − 3000 km/s). The 2000 − 3000 km/s shells contains very little oxygen in order to reproduce the narrow peak on top of the [O I] λλ 6300,6363 doublet lines and therefore it has low optical depth. Apart from the innermost shell, the optical depth drops below one around 220 days. This optical depth is calculated for scattering of remote emission radiation, which has a weaker dependence on the clumping factor than for local scattering.

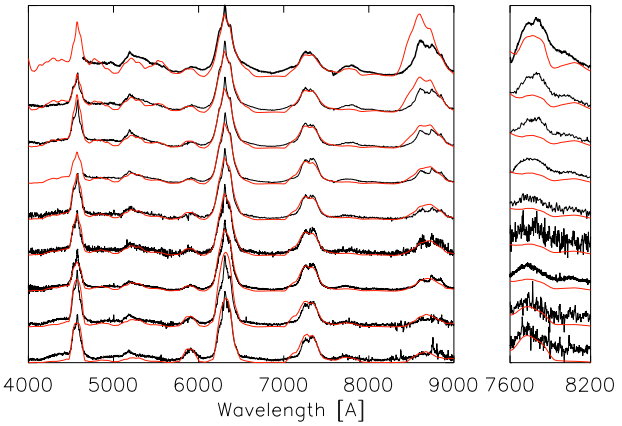

Figure 7. SN 2002ap, models for a clumping factor $\zeta = 25$. Left side: normalised nebular spectra (from top to bottom: 129, 163, 192, 229, 245, 253, 281, 343 and 394 days after explosion) are shown in black with synthetic spectra in red. Right side: the region between 7600 Å and 8200 Å is enlarged to enable a comparison of observed (black) and synthetic (red) 7774 Å flux. At epochs of 129 and 163 days, the simulated flux matches the observations at 7774 Å much better than for low clumping factors but in general the fit to the forbidden line emission is worse (e.g. the [O I] 5577 Å line and the Ca II IR-triplet line at $\sim$ 8500 Å become too strong at early epochs). Around 200 days line scattering seems necessary to explain the observed 7774 Å flux.

Maeda et al. 2006). While Mazzali et al. (2001) attempted to model individual nebular spectra by one-zone models (concluding that this is insufficient), Maeda et al. (2006) computed two-dimensional synthetic nebular spectra for models obtained from hydrodynamical simulations, finding good agreement with spectra of individual epochs. However no model has so far described the time sequence of nebular spectra of SN 1998bw consistently.

In this section we try to find a single two-dimensional model which is consistent with the full time evolution from 108 to 388 days after explosion. While successful models for individual epochs can be found even in one dimensional modelling, it seems impossible to model the time sequence of all spectra with a single one-dimensional model (in contrast to SN 2002ap, where this approach works well).

Since SN 1998bw is quite massive compared to other CC-SNe (like SN 2002ap for example), the transition to the nebular phase occurs at rather late times, although the ejecta expand at high velocities. The spectra at 108 and 139 days after explosion are not strictly nebular and therefore large deviations between the model and the observations are to be expected when trying to reproduce these spectra (especially at 108 days) with our nebular code.

When considering two dimensions one is immediately confronted with the problem that the parameter space is much larger [angular distribution of elements, observer inclination]. In addition, the computation time to obtain one synthetic spectrum increases dramatically. Since hundreds of spectra have to be computed to obtain a good model, this technical problem can make modelling unfeasible. Therefore some assumptions about the SN geometry have to be introduced.

There are several good arguments to assume that SN 1998bw might consist of some kind of two-dimensional 'jet + disc' structure, as described by for example by Maeda et al. (2006) (see Section 1). Furthermore, since the SN was accompanied by a GRB, it seems likely that the observer inclination is not too far from polar, although this is uncertain since the opening angle of GRB 980425 is not known.

Therefore we work with a parametrised two-dimensional model which consists of a polar zone (0° to 45°) and an equatorial zone (45° to 90°). This simplification will introduce some error, since most likely it does not represent physical reality. However, it seems sufficiently exact to obtain an acceptable fit at all epochs with a single ^{56}Ni/O model. A model with more degrees of freedom is highly degenerate anyway, since the information that can be extracted from a series of spectra F(ν,t) is limited.

Because of this simplification the reliability of our model is in question, but this kind of uncertainty is inherent to all multi-dimensional modelling. We performed tests for viewing angles of 0°, 15° and 30°. Using the smaller viewing angles the iron lines which are mainly produced in the jet-like structure become very narrow, which is not observed. Therefore we decided to use a viewing angle of 30°. However this might be a consequence of our simplified geometry and therefore it is not possible to obtain valuable information about the observers inclination from our modelling approach.

Our model is roughly consistent with previous findings (Maeda et al. 2006). The polar zone contains $\sim$ 0.24 M$_\odot$ of ^{56}Ni at velocities below 12000 km/s. The equatorial zone also contains $\sim$ 0.24 M$_\odot$ of ^{56}Ni (note that the equatorial zone has more than twice the surface area of the polar zone), but located at velocities below $\sim$ 8000 km/s. The total mass below 12000 km/s is estimated to be $\sim$ 2.7 M$_\odot$ containing a total oxygen mass (below 12000 km/s) of $\sim$ 2 M$_\odot$. There is a lot of material at higher velocities, but the nebular modelling becomes inaccurate for the outer regions because the density is too low.

Again we find that the O I 7774 Å line is not reproduced as due to recombination by our model with clumping $\zeta = 1$ and $\zeta = 5$. Mazzali et al. (2001) and Maeda et al. (2006) had used a clumping factor of 10. This will be discussed in Section 5] for the spectra at 108, 139 and 214 days (see Figures 8 and 10). At 349 and 388 days we can reproduce the O I 7774 Å line consistently with the observations. There is some background around 7774 Å which is not reproduced by the nebular code sufficiently exactly. Shifting the oxygen recombination line upwards by the possible background, the agreement seems reasonable for both clumping factors. However the large background-line ratio makes an exact comparison impossible.

We tried to explain the formation of O I 7774 Å at the earlier epochs (108, 139 days) by increasing the clumping factor, which in turn increases the thermal electron excitation from the 3s(^{5}S) to the 3p(^{5}P) level. However, this does not seem to work. Both [O I] 5577 Å and the Ca II IR-triplet become very strong at clumping factors > 10, while the synthetic flux around 7774 Å increases but seems still too weak to explain the observations. Owing to the high density of SN 1998bw the nebular approach might be not suitable for such early epochs (the strong continuum which is observed is not reproduced). In addition there are uncertainties on

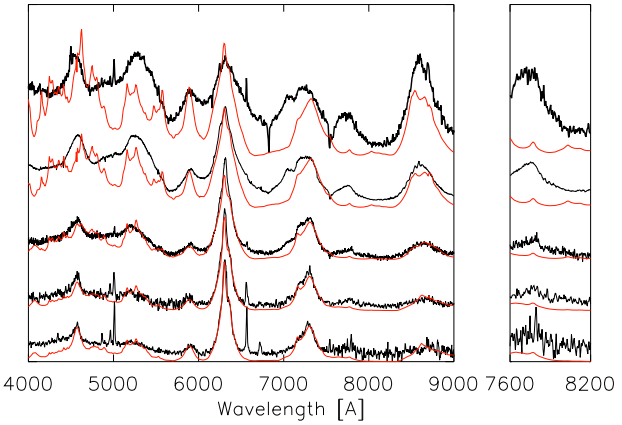

Figure 8. SN 1998bw, case of no clumping ($\zeta = 1$). Left side: normalised nebular spectra of SN 1998bw (from top to bottom: 108, 139, 214, 349 and 388 days after explosion) are shown in black with the synthetic spectra in red. On the right side the region between 7600 Å and 8200 Å is enlarged to enable a comparison of observed (black) and synthetic (red) 7774 Å flux. The two earliest spectra (108, 139 days) of SN 1999bw are clearly not nebular and the agreement between observations and simulations is expected to be poor. However, the evolution of total and oxygen 6300 Å flux as well as the shape of the [O I] $\lambda\lambda$ 6300,6363 doublet line are reproduced at all epochs much better than by a one-dimensional model. At epochs of 108 to 349 days, the simulated flux is too low to match the observations of the 7774 Å line. At 388 days, considering the constant offset caused by some background flux which is not reproduced by the synthetic spectrum, the synthetic 7774 Å line seems to be consistent with the observations. Unfortunately the noise level is high and a detailed comparison is not possible.

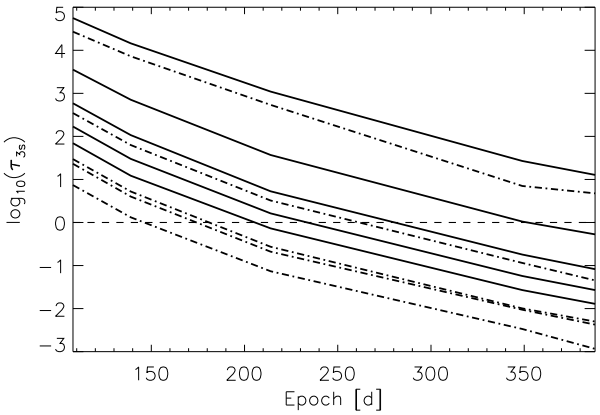

Figure 9. SN 1998bw, case of no clumping ($\zeta = 1$). The logarithm of the 7774 Å line optical depth in our model for the inner shells (from top to bottom: 0 − 1000 km/s, 1000 − 2000 km/s, 2000 − 3000 km/s, 3000 − 4000 km/s and 4000 − 5000 km/s). Solid lines show the equatorial region, dotted lines the polar region. Apart from the innermost shell, the optical depth drops below one at $\sim$ 210 days. This optical depth is calculated for scattering remote emission radiation, which has a weaker dependence on the clumping factor than for local scattering.

the atomic data (especially the collision strengths), which may influence our conclusion.

In Figures 9 and 11 we show the opacity of the 7774 Å line for the five innermost shells for clumping factors of $\zeta = 1$ and $\zeta = 5$. There will be 7774 Å line absorption up to $\sim 200 - 300$ days depending on clumping.

Again, at least moderate clumping ($\zeta \sim 5$) seems necessary in order to provide enough O I 7774 Å line opacity to reproduce the observations at 214 days.

5 DISCUSSION

In Section 2.1 we have obtained normalised effective recombination fractions using available atomic data and computing missing atomic data. The agreement with atomic data available in the literature is good. Effective recombination rates had been given before by Julienne et al. (1974) at a temperature of 1160 K. These results are reproduced well. We extend the temperature range up to 10000 K, which should be an upper limit for temperatures of SN nebular ejecta between 100 and 600 days. Typical uncertainties in the atomic data seem to have small influence.

In Sections 2.2 and 2.3 we have obtained estimates for the formation of oxygen recombination lines and line absorption by the 3s(^{5}S) state of neutral oxygen. We have shown that the luminosity of recombination lines is weak at any

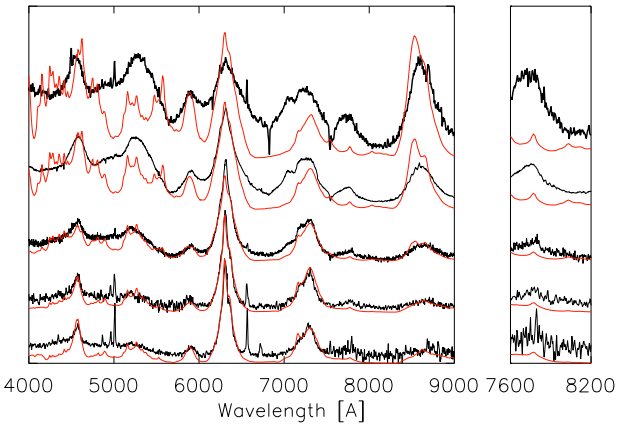

Figure 10. SN 1998bw, case of clumping ($\zeta = 5$). Left side: normalised nebular spectra (from top to bottom: 108, 139, 214, 349 and 388 days after explosion) are shown in black with the synthetic spectra in red. Right side: the region between 7600 Å and 8200 Å is enlarged to enable a comparison of observed (black) and synthetic (red) 7774 Å flux. The two earliest spectra (108, 139 days) of SN 1999bw are clearly not nebular and the agreement between observations and simulations is expected to be poor. However, the evolution of total and oxygen 6300 Å flux as well as the shape of the [O I] $\lambda\lambda$ 6300,6363 doublet line are reproduced at all epochs much better than by a one-dimensional model. At epochs of 108 to 349 days, the simulated flux is too low to match the observations of the 7774 Å line. At 388 days, considering the constant offset caused by some background flux which is not reproduced by the synthetic spectrum, the synthetic 7774 Å line seems to be consistent with the observations. Unfortunately the noise level is rather high and a detailed comparison is not possible.

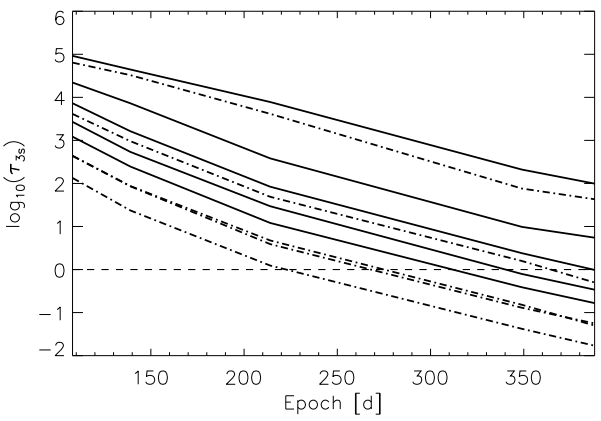

Figure 11. SN 1998bw, case of clumping ($\zeta = 5$). The logarithm of the 7774 Å line optical depth of our ejecta model for the inner shells (from top to bottom: 0 - 1000 km/s, 1000 - 2000 km/s, 2000 - 3000 km/s, 3000 - 4000 km/s and 4000 - 5000 km/s). Solid lines show the equatorial region, dotted lines the polar region. Apart from the innermost shell, the optical depth drops below one at $\sim$ 310 days. This optical depth is calculated for scattering remote emission radiation, which has a weaker dependence on the clumping factor than for local scattering.

epoch. The influence of clumping on the recombination line is weak as well. Clumping will increase the recombination rate, but will decrease the number of O II ions at the same time. The total number of recombinations, which is equivalent to the total number of ionisations, will increase only slightly. Therefore clumping offers no direct way for increasing O I 7774 Å emission considerably.

We have shown that there is line scattering of 7774 Å photons even at very late epochs. This is possible because of the large number of ground state O I atoms, which resonantly scatter the UV radiation emerging from 3s to 2p transitions and slow down the de-population of the 3s state. Combined with recombination this leads to a high population of the 3s level, which in turn can resonantly scatter 7774 Å radiation. We have shown that, in contrast to the direct recombination line, the scattering line is very sensitive to clumping of the ejecta.

In addition, for high clumping factors, there may be thermal electron collisional excitation of the O I 7774 Å line at early epochs. However, it is in question whether these high clumping factors are realistic since high density lines, which are not observed, may form. Uncertainties in the atomic data, especially the collision strengths, may influence our results.

The considerations regarding the O I 7774 Å line are also in principle valid for the [O I] 8446 Å line [3s(^{3}S) to 2p(^{3}P)] with the difference that the effective recombination rate into the 3s triplet state is smaller than into the quintet state. The optical depth of the 8446 Å line is therefore expected to be lower, which is still sufficient to cause line scattering at very early epochs. However, the 8446 Å line is blended with the blue wing of the [Ca II] IR-triplet, which can explain why no [O I] 8446 Å line is identified in SNe 1998bw and 2002ap.

We have shown that there is likely to be no other effective excitation mechanism than 'recombination + thermal excitation' or 'recombination + absorption' for O I $n \geqslant 3$ levels. Thermal electron excitation of $n \geqslant 3$ levels from the ground level is ineffective at typical nebular temperatures. Non-thermal electron excitation can also be ruled out. First, it is too weak and second, it would produce a temporal behaviour of the O I 7774 Å line which is not observed. As detailed modelling showed (Sections 3 and 4) absorption might be too weak to explain the observations as long as there is no clumping of the ejecta ($\zeta \sim 5$). To enable thermal electron excitation even larger clumping factors seem necessary.

The concept of clumping has often been used in stellar wind and SN radiation physics (e.g. Li & McCray 1992, 1993; Mazzali et al. 2001; Maeda et al. 2006; Mazzali et al. 2007a) without quantitative understanding of the physics behind ejecta clumping, therefore playing the role of a fitting factor. Li & McCray (1992) have modelled the ratio of the [O I] $\lambda\lambda$ 6300, 6363 doublet lines and Li & McCray (1993) the Ca II emission of SN 1987A using a clumping factor of $\sim$ 10. Mazzali et al. (2001); Maeda et al. (2006); Mazzali et al. (2007a) have modelled the nebular spectra of SNe 1998bw and 2002ap finding that better fits to observations are obtained using clumping factors of $\sim$ 10 than when using no clumping. Our results are similar, but show some difference. We obtain good fits to all forbidden lines using clumping factors of 1 and 5 as well. The abundance of elements will change slightly depending on the value chosen. We even found a slight decrease in the quality of the fit when going from $\zeta = 5$ to $\zeta = 10$ and therefore we used the lower value. This difference probably results mainly from our more accurate treatment of ionisation which increases the ionisation rate of carbon and oxygen considerably. This means that the electron density is increased, which can be mimiced by increasing the clumping factor and using lower ionisation rates. It might also be partially attributed to the fact that there is no strict criterion for the quality of a fit for nebular spectra.

Still, the constraints we derived for the clumping factor of SNe 1998bw and 2002ap from the O I 7774 Å scattering line compare well to previous findings. We found that a clumping factor of $\sim$ 5 seems necessary to provide sufficient opacity at 7774 Å. Clumping factors of $\zeta > 10$ make it possible to model the O I 7774 Å emission at early epochs without line scattering, but may cause the formation of high density emission lines at early epochs (100 − 150 days). One example is the [O I] 5577 Å singlet line, which is observed to be weak. Since there are uncertainties on the atomic data it is not clear whether thermal electron excitation is important and whether the O I 7774 Å line at early epochs is dominated by line scattering or thermal electron excitation of recombining electrons.

At later epochs, between 150 and 250 days, the line is most likely a combination of line scattering and recombination radiation, since thermal electron excitation becomes too weak for any reasonable value of clumping. Around $\sim$ 250 days the O I 7774 Å line seems to become a true recombination line where the flux is mainly provided by the electrons cascading into the 3p(^{5}P) level.

In Section 2.4 we have studied the expected profile of the [O I] 7774 Å line in light of our previous findings. As expected, the absorption and emission line shapes caused by a certain ejecta distribution can show important differences.

Further, the profile of the absorption line depends on the background radiation field and one should be careful when using the shape of a scattering line for any kind of argumentation about ejecta geometry as long as it not clear how this line is formed in detail.

In Sections 3 and 4 we obtained core ejecta models for SNe 1998bw and 2002ap. The primary goal of this modelling was not to re-derive ejecta properties, but to obtain reliable models for studying oxygen recombination consistently with other line formation.

As a by-product we obtained estimates for the ^{56}Ni and oxygen masses of the cores of these SNe. We find that SN 2002ap can be described very well by a one-dimensional shell model (as already found before), which does not necessarily mean that there is no asymmetry. Our ^{56}Ni ($\sim$ 0.07 M$_\odot$) and oxygen mass estimates seem consistent with previous work. For SN 1998bw one-dimensional modelling seems to be insufficient to obtain an acceptable fit at all epochs using a single model. An acceptable fit is obtained with a two-dimensional 'jet + disc' model (this had been found before). The fit could certainly be improved by increasing the degree of freedom of the model, but this would become extremely time-consuming. The model found in this work reproduces the observations at all epochs with increasing accuracy at later times, which is expected. The estimate of the ^{56}Ni ($\sim$ 0.48 M$_\odot$) and oxygen mass are consistent with previous results.

Using these ejecta distributions we were able to reproduce the formation of O I 7774 Å at late epochs. There is enough line opacity at 7774 Å at early and intermediate nebular epochs to produce a strong scattering line. Since the background radiation field is important for the calculation of this absorption line, we were not able to show that our ejecta distribution reproduces the observations at early epochs exactly, however this seems likely. If there is strong clumping the O I 7774 Å line may be additionally excited by thermal electrons. The oxygen distribution inferred from forbidden line observations allows the reproduction of the allowed oxygen lines at late epochs. Since different physics are involved, this provides a test for the consistency of the nebular modelling approach, which is passed for SNe 1998bw and 2002ap.

Several other ions may produce absorption lines at wavelengths between 4000 and 10000 Å (the part of the spectrum that is usually observed). Since the abundance of these elements is much lower than that of oxygen, there will be no excited states with sufficient population to cause significant line scattering (an exception might be the Ca II IR-triplet). Allowed ground state transitions with energies between $\sim$ 1 and 3 eV are interesting since their optical depth can be high owing to the high radiative rates of allowed lines and to the possibly sufficiently high ground state populations of these low abundance elements. The elements of interest are Na I, Mg I and Ca II. These three elements have low quantum-level transitions with wavelengths of $\sim$ 5890 Å (Na I) , 4570 Å (Mg I) and 3950 Å , 7300 Å and 8500 Å (Ca II), which can be present in sufficient amounts in SN nebulae. Iron group element lines, especially Fe II, may be optically thick as well. However, since these ions are complex we do not treat them explicitly here.

If 0.01 M$_\odot$ of Na I were to be distributed homogeneously within 5000 km/s, the optical depth of the Na I 5890 Å line would be $\sim 6 \times 10^5$ at 200 days (this result is obtained by balancing thermal-electron excitation with radiative and collisional de-excitation analogously to Section 2.2), scaling linearly with Na I mass and with epoch t^{-2}.

If 0.01 M$_\odot$ of Mg I were to be distributed homogeneously within 5000 km/s, the optical depth of the Mg I] 4570 Å line would be $\sim$ 1 at 200 days, scaling linearly with Mg I mass and with epoch t^{-2}.

Three Ca II lines might be seen in absorption even at late epochs ($\sim$ 3950 Å, 7300 Å and the IR-triplet 8500 Å). To estimate their strength, it is important to know the relative population of the Ca II 3d to 4s states, which can be approximated by

$$\frac{n_{3d}}{n_{4s}} \sim \frac{C_{4s\rightarrow 3d}}{A'_{3d\rightarrow 4s} + C_{3d\rightarrow 4s}} \qquad (20)$$

where $C_{4s\rightarrow 3d}$ and $C_{3d\rightarrow 4s}$ are the collisional rates for the 4s to 3d transition and A' is the radiative rate from 3d to 4s, reduced due to resonance scattering.

If 0.01 M$_\odot$ of Ca II were to be distributed homogeneously within 5000 km/s, the optical depth of the Ca II 3950 Å and [Ca II] 7300 Å lines would be $\sim 2 \times 10^5$ and $\sim$ 0.02 respectively, at 200 days, scaling linearly with the Ca II mass and with epoch t^{-2}. The optical depth of the Ca II IR-triplet depends on the population of the 3d state. Using the 7300 Å optical depth estimated above, the optical depth of the Ca II 8500 Å transition is $\sim$ 430 ($n_e = 10^7$ and T = 5000 K) at 200 days, with a stronger dependence on Ca II mass and epoch than the optical depths at 3950 Å and 8500 Å (see also Li & McCray 1993, for a detailed discussion of Ca II line formation) .

The exact mass of Na I, Mg I and Ca II is not well known, since estimates of their masses are not very accurate. However, typical masses in CC-SNe cores for Na, Mg and Ca might be of the order of 0.01 M$_\odot$.

Therefore, even at late times (> 200 days) there is strong line scattering at wavelengths between $\sim$ 4000 and 10000 Å. The Ca II 3950 Å, Na I 5890 Å and O I 7774 Å lines cause strong scattering in any reasonable scenario. The [Mg I] 4570 Å, O I 8446 Å and Ca II 8500 Å lines may have sufficient optical depth for line scattering, depending on epoch, degree of ionisation, total mass and clumping.

6 SUMMARY AND CONCLUSION

We have computed temperature-dependent effective recombination rates for neutral oxygen in a temperature range suitable for all types of SN nebulae (at epochs between 100 and 600 days). Since oxygen is the most abundant element in stripped-envelope CC-SNe, oxygen lines are of special interest among other recombination lines.

We obtained core ejecta models for CC-SNe 1998bw and 2002ap. Similar models had been derived previously. Using these oxygen profiles, the O I 7774 Å recombination line, which is the strongest observed recombination line, is calculated and compared to observations. We show that up to late epochs pure recombination is too weak to power O I 7774 Å. At earlier epochs the line is powered by scattering and possibly by thermal electron excitation of recombining electrons. In both scenarios the population of the 3s(^{5}S) state by recombining electrons is the key to the O I 7774 Å emission.

We derived estimates for the strength of the O I 7774 Å line resulting from oxygen recombination, for the time-dependent optical depth of this line and for excitation of recombining electrons by thermal collisions. These estimates give insight into the formation of the O I 7774 Å line in CC-SNe. We have shown that while the recombination line strength depends on clumping very weakly, clumping does have a strong influence on the absorption and thermal electron excitation of this line.

Constraints on the clumping factor have been rare so far. A common choice is a value of $\zeta \sim 10$, consistent with the findings of this paper. At the current level of accuracy it is only possible to set upper and lower limits to the clumping factor ($100 \gg \zeta > 1$).

Our results imply that the [O I] 7774 Å line should not be used as a tracer of the core ejecta before 250 days, unless one explicitly models the background radiation field and the recombination and absorption processes involved. Since the clumping factor can not be obtained with high accuracy and the background around 7774 Å seems to consist of a superposition of several weak lines this could become a difficult task. It is not clear which elements or ions produce the observed background flux in this region. Iron group elements seem to be promising candidates, but currently the accuracy of our calculations is not sufficient.

ACKNOWLEDGMENTS

We thank Keith Butler for reading the manuscript and for making useful comments.

REFERENCES

Aldrovandi S. M. V., Pequignot D., 1973, A&A, 25, 137
Axelrod T. S., 1980, Ph.D. thesis, AA(California Univ., Santa Cruz.)
Badnell N. R., 2006, ApJS, 167, 334
Bates D. R., Damgaard A., 1949, Philosophical Transactions of the Royal Society of London. Series A, Mathematical and Physical Sciences, 242, 842, 101
Bell K. L., Hibbert A., 1990, J. Phys. B: At. Mol. Opt. Phys., 23, 2673
Bhatia A. K., Kastner S. O., 1995, ApJS, 96, 325
Blondin J. M., Mezzacappa A., DeMarino C., 2003, ApJ, 584, 971
Burgess A., Seaton M. J., 1960, MNRAS, 120, 121
Burke P. G., Robb W. D., 1975, Advances in Atomic and Molecular Physics, vol. 11, ACADEMIC PRESS New York, 111 Fifth Aveneu, New York, New York 10003
Burrows A., Livne E., Dessart L., Ott C. D., Murphy J., 2007, ApJ, 655, 416
Chung S., Lin C. C., Lee E. T. P., 1991, Phys. Rev. A, 43, 7, 3433
Filippenko A. V., 1997, ARA&A, 35, 309
Galama T. J., Vreeswijk P. M., van Paradijs J., et al., 1999, A&AS, 138, 465
Höflich P., 1991, A&A, 246, 481
Höflich P., Wheeler J. C., Wang L., 1999, ApJ, 521, 179
Iwamoto K., Mazzali P. A., Nomoto K., et al., 1998, Nature, 395, 672
Julienne P., Davis J., Oran E., 1974, J. Geophys. Res., 79, 16, 2540
Kay L. E., Halpern J. P., Leighly K. M., et al., 1998, in Bulletin of the American Astronomical Society, vol. 30 of Bulletin of the American Astronomical Society, 1323–+
Kotake K., Sawai H., Yamada S., Sato K., 2004, ApJ, 608, 391
Lennon M. A., Bell K. L., Gilbody H. B., et al., 1988, J.Phys.Chem.Ref.Data, 17, 3, 1285
Li H., McCray R., 1992, ApJ, 387, 309
Li H., McCray R., 1993, ApJ, 405, 730
Lotz W., 1967, ApJS, 14, 207
Lotz W., 1970, J. Opt. Soc. Am., 60, 2, 206
Lucy L. B., 1991, ApJ, 383, 308
Maeda K., Kawabata K., Tanaka M., et al., 2007a, ApJ, 658, L5
Maeda K., Nakamura T., Nomoto K., Mazzali P. A., Patat F., Hachisu I., 2002, ApJ, 565, 405
Maeda K., Nomoto K., Mazzali P. A., Deng J., 2006, ApJ, 640, 854
Maeda K., Tanaka M., Nomoto K., et al., 2007b, ApJ, 666, 1069
Malesani D., Tagliaferri G., Chincarini G., et al., 2004, ApJ, 609, L5
Matheson T., 2004, in Cosmic explosions in three dimensions, edited by P. Höflich, P. Kumar, J. C. Wheeler, 351–+
Maurer J. I., Mazzali P. A., Deng J., et al., 2009, MNRAS, 1825–+
Mazzali P. A., Deng J., Maeda K., et al., 2002, ApJ, 572, L61
Mazzali P. A., Deng J., Maeda K., Nomoto K., Filippenko A. V., Matheson T., 2004, ApJ, 614, 858
Mazzali P. A., Kawabata K. S., Maeda K., et al., 2005, Science, 308, 1284
Mazzali P. A., Kawabata K. S., Maeda K., et al., 2007a, ApJ, 670, 592
Mazzali P. A., Nomoto K., Patat F., Maeda K., 2001, ApJ, 559, 1047
Mazzali P. A., Röpke F. K., Benetti S., Hillebrandt W., 2007b, Science, 315, 825
Mazzali P. A., Valenti S., Della Valle M., et al., 2008, Science, 321, 1185
Moiseenko S. G., Bisnovatyi-Kogan G. S., Ardeljan N. V., 2006, MNRAS, 370, 501
Nakamura T., Maeda K., Iwamoto K., et al., 2000, in Highly Energetic Physical Processes and Mechanisms for Emission from Astrophysical Plasmas, edited by P. C. H. Martens, S. Tsuruta, M. A. Weber, vol. 195 of IAU Symposium, 347–+
Nussbaumer H., Storey P. J., 1983, A&A, 126, 75
Patat F., Cappellaro E., Danziger J., et al., 2001, ApJ, 555, 900
Pequignot D., 1990, A&A, 231, 499
Pian E., Mazzali P. A., Masetti N., et al., 2006, Nature, 442, 1011
Ralchenko Y., Janev R. K., Kato T., Fursa D. V., Bray I., de Heer F. J., 2008, Atomic Data and Nuclear Data Tables, 94, 603
Rozsnyai B. F., Jacobs V. L., Davis J., 1980, Phys. Rev. A, 21, 6, 1798
Sauer D. N., Mazzali P. A., Deng J., Valenti S., Nomoto

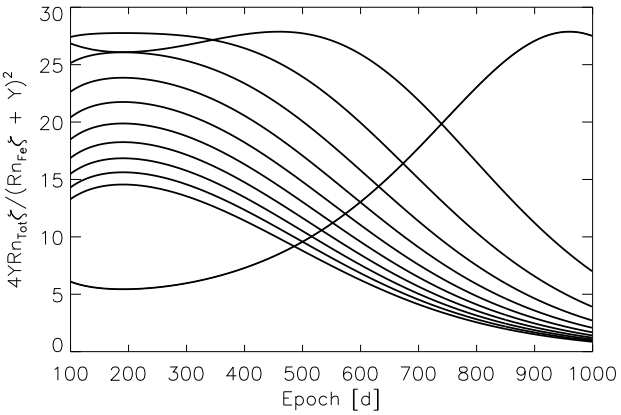

Figure 12. The ratio $4Y'_{\rm O[I]}R_{\rm O[I]}n_{\rm Tot}\zeta/(R_{\rm O[I]}n_{\rm Fe}\zeta + Y'_{\rm O[I]})^2$ for different clumping factors (ζ = 1, 10, 20, 30, 40, 50, 60, 70, 80, 90 and 100 from top to bottom) at 1000 days calculated for the same model as used in Figures 3,13 and 14. For this model the ratio is much larger than one for any reasonable clumping factor (1 - 100) at epochs earlier than 600 days.

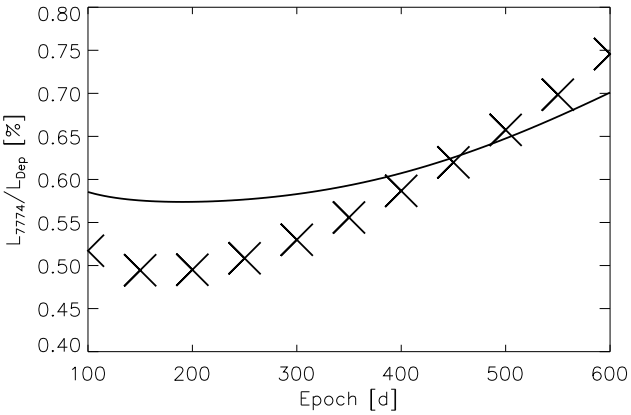

Figure 13. The solid line is a computation of Equation 9 performed for the O I 7774 Å line assuming a constant temperature of 4000 K at all epochs for the one-zone model described in the text. The luminosity of this line is compared to the total deposited luminosity. The results are given in %. The recycling fraction was set to the ratio of ground state to total recombination rate at 4000 K. The crosses show data points obtained with the nebular code for the same model, where the temperature is computed at all epochs self-consistently and ionisation is treated in detail. Considering the large change of the temperature between 100 and 600 days (6800 K and 2800 K respectively) the agreement seems reasonable (note that the temperature calculated by the code drops below 4000 K around 450 days). The minimum around 200 days is present in both curves.

K., Filippenko A. V., 2006, MNRAS, 369, 1939
Seaton M. J., 1958, MNRAS, 118, 504
Storey P. J., Hummer D. G., 1995, MNRAS, 272, 41
Stritzinger M., Mazzali P. A., Sollerman J., Benetti S., 2006, A&A, 460, 793
Takiwaki T., Kotake K., Sato K., 2009, ApJ, 691, 1360
Taubenberger S., Valenti S., Benetti S., et al., 2009, MNRAS, 397, 677
van Regemorter H., 1962, ApJ, 136, 906
Woosley S. E., Bloom J. S., 2006, ARA&A, 44, 507
Xu Y., McCray R., 1991, ApJ, 375, 190
Yoshii Y., Tomita H., Kobayashi Y., et al., 2003, ApJ, 592, 467

APPENDIX A

In Section 2.2 and 2.3 we have derived several estimates for quantities relevant for calculating O I 7774 Å nebular emission. To derive these estimates, we used some approximations. These are justified here by comparison to results from the nebular code, which are not based on these approximations and will show deviations as soon as our approximations fail. An important difference is introduced by the temperature. While the electron temperature is calculated considering hundreds of emission lines in the nebular code, this is not possible for our estimates and we use a temperature of 4000 K for the calculations.

To perform these tests we set up a test one-zone model with a total mass $M_{\rm Tot} \sim 0.5$ $M_\odot$, an expansion velocity of 5000 km/s, containing 80% oxygen, 10% ^{56}Ni, $\sim$ 9% carbon, and other elements like calcium, magnesium and sodium.

Usually one can assume $4Y'_{\rm O[I]}R_{\rm O[I]}n_{\rm Tot}\zeta/(R_{\rm O[I]}n_{\rm Fe}\zeta + Y'_{\rm O[I]})^2 \gg 1$, which depends on the iron to oxygen ratio, the deposited luminosity, the electron temperature and the clumping factor. In Figure 12 we show this ratio for our test model using clumping factors of one to one hundred. At any

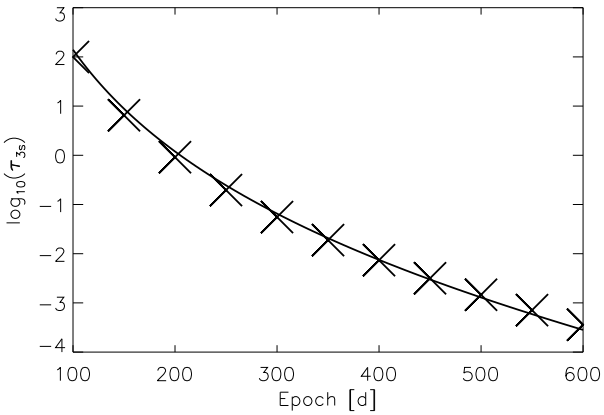

Figure 14. The solid line shows a computation of Equation 14 performed for the logarithmic line opacity of the O I 7774 Å line assuming a constant temperature of 4000 K at all epochs for a one-zone model described in the text. The crosses show data points obtained with the nebular code for the same model, where the temperature is computed at all epochs self-consistently and ionisation is treated in detail. The agreement is good, especially around 450 days, when the simulated temperature drops below 4000 K, which we assumed in our calculation. The line optical depth is greater than one until day $\sim$ 200.

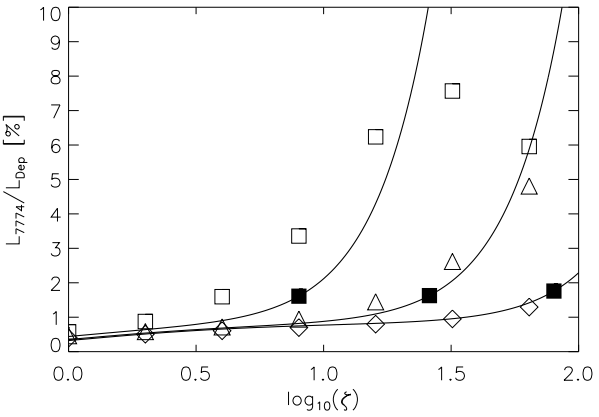

Figure 15. The O I 7774 Å line luminosity from pure recombination and thermal excitation of recombining electrons relative to the total deposited luminosity in % for the test models described in the text using clumping factors between 1 and 100. Solid lines show estimates obtained from Equations 9 and 17 for oxygen densities of 10^7, $10^{7.5}$ and 10^8 cm^{-3} from bottom to top. Results from our nebular code are shown by diamonds (10^7 cm^{-3}), triangles ($10^{7.5}$ cm^{-3}) and squares (10^8 cm^{-3}). The agreement is good. Small deviations are predominately caused by our rough approximation of the temperature. Filled squares mark $n_{\rm O}\zeta \sim 10^9$ cm^{-3} where our estimates are expected to become inaccurate. At $n_{\rm O}\zeta > 10^{9.3}$ cm^{-3} our approximation breaks down completely, but this regime is probably not important for the nebular phase of stripped CC-SNe. The 7774 Å luminosity increases with the increasing clumping until the density becomes high enough to depopulate the 3s(^{5}S) state by thermal electron collisions effectively.

epoch of interest (100 to 600 days) and for any clumping factor the assumption is valid. The assumption may fail for clumping factors ~ 1 at lower densities and for higher ^{56}Ni to oxygen ratios. For clumping factors $\zeta \gg 1$ the assumption will hold for any plausible CC-SN scenario.

In Figures 13 and 14 we compare Equations 9 and 14 (temperature set to T = 4000 K) with the results obtained from our nebular code using our test model. The temperature is kept constant in the calculation, while it is calculated self-consistently in the nebular code, influencing the recombination fraction and recombination rate. Also the ionisation of ions other than O I and Fe I has been neglected in the calculation. Despite the approximations, the agreement seems reasonable.

In Figure 15 we compare the O I 7774 Å flux from pure recombination and electron scattering of recombining electrons (Equations 9 and 17) to results obtained from our nebular code using variations of our test model. We set the epoch to 150 days and use oxygen densities of 10^7, $10^{7.5}$ and 10^8 cm^{-3}, which should cover the range expected for stripped CC-SNe. The oxygen fraction is again set to 80%. For our estimates we use a temperature of 5000 K (the temperature calculated by the nebular code varies between 4500 K and 6300 K for these models). The breakdown point of our estimate ($n_{\rm O}\zeta > 10^9$ cm^{-3}) is indicated by filled squares. Up to the breakdown point the agreement is good. For larger clumping factors the agreement is acceptable for $n_{\rm O}\zeta < 10^{9.3}$ cm^{-3}. For larger clumping factors our estimate over predicts the 7774 Å luminosity. In this regime the population of the 3s(^{5}S) level is no longer controlled by the effective radiative rate but rather by collisional de-excitation by thermal electrons. It seems unlikely that such high density regimes can play a role in CC-SN nebulae.

APPENDIX B

Normalised effective recombination fractions for triplet and quinted states of O I n = 3. For the triplet states we show calculations for the cases of optical thin * and thick ground states. These numbers have to be multiplied by the total radiative recombination rate to obtain the effective recombination rates. Since the total radiative recombination rate also contains a direct ground state component and since lower levels contain cascade contributions from the higher levels these fractions do not add up to one.

At high densities, collisional transitions become important, which are not included in our cascade calculation. At densities $n_{\rm e} < 10^{10}$ cm^{-3} and temperatures of $T \sim 5000$K the error on the recombination rates owing to this effect should be less than 10%.

At high temperatures di-electronic recombination becomes important, while at low temperature and high densities collisional recombination can become important. Under nebular conditions both effects should be of the order of 10% or less.

To obtain the effective recombination coefficient for a certain line one has to weigh the upper level by the corresponding radiative rates[3]. As an example, we calculate the normalised effective recombination coefficient f_{6157} of the quinted 4d(^{5}D) $\rightarrow$ 3p(^{5}P) 6157 Å line at 1000K. The radiative rate from 4d(^{5}D) to 3p(^{5}P) is given by $A_{6157} = 7.62(+6)$ s^{-1} and the radiative rate 4d(^{5}D) to 4p(^{5}P) is given by $A_{26511} = 6.44(+6)$ s^{-1} and therefore

$$f_{6157} = f_{4{\rm d}(^5{\rm D})} \frac{A_{6157}}{A_{6157} + A_{26511}} = 3.8(-2) \qquad (21)$$

which agrees well with the value given by Julienne et al. (1974) at 1160K.

[3] http://www.nist.gov/index.html

Table 1. Effective normalised recombination fraction of O I for triplet and quinted states of O I n = 3. The rates are normalised on the total radiative recombination rate of Badnell (2006). States indicated by * show the case of optical thin ground state transitions. Values in brackets indicate a power of 10, e.g. a(b) = a · 10^b.

State	1000K	2000K	3000K	4000K	5000K	6000K	7000K	8000K	9000K	10000K
3s(^{3}S)*	4.6(-2)	4.2(-2)	4.0(-2)	3.8(-2)	3.7(-2)	3.6(-2)	3.4(-2)	3.3(-2)	3.2(-2)	3.1(-2)
3p(^{3}P)*	4.3(-2)	4.0(-2)	3.8(-2)	3.6(-2)	3.5(-2)	3.4(-2)	3.2(-2)	3.0(-2)	2.9(-2)	2.8(-2)
3d(^{3}D)*	1.6(-1)	1.4(-2)	1.3(-1)	1.2(-1)	1.1(-1)	1.1(-1)	1.0(-1)	9.4(-2)	8.9(-2)	8.5(-2)
3s(^{3}S)	2.7(-1)	2.5(-1)	2.4(-1)	2.3(-1)	2.2(-1)	2.1(-1)	2.0(-1)	1.9(-1)	1.8(-1)	1.7(-1)
3p(^{3}P)	2.6(-1)	2.4(-1)	2.3(-1)	2.1(-1)	2.0(-1)	2.0(-1)	1.9(-1)	1.8(-1)	1.7(-1)	1.6(-1)
3d(^{3}D)	1.7(-1)	1.5(-1)	1.4(-1)	1.3(-1)	1.2(-1)	1.2(-1)	1.1(-1)	1.0(-1)	9.8(-2)	9.3(-2)
3s(^{5}S)	4.7(-1)	4.5(-1)	4.3(-1)	4.1(-1)	3.9(-1)	3.8(-1)	3.6(-1)	3.5(-1)	3.3(-1)	3.2(-1)
3p(^{5}P)	4.6(-1)	4.3(-1)	4.1(-1)	3.9(-1)	3.8(-1)	3.6(-1)	3.5(-1)	3.3(-1)	3.2(-1)	3.0(-1)
3d(^{5}D)	2.7(-1)	2.4(-1)	2.2(-1)	2.1(-1)	1.9(-1)	1.8(-1)	1.7(-1)	1.6(-1)	1.5(-1)	1.5(-1)
4s(^{3}S)*	6.9(-3)	7.0(-3)	7.0(-3)	6.8(-3)	6.6(-3)	6.4(-3)	6.2(-3)	6.0(-3)	5.7(-3)	5.5(-3)
4p(^{3}P)*	9.0(-3)	9.1(-3)	9.0(-3)	8.7(-3)	8.4(-3)	8.1(-3)	7.8(-3)	7.5(-3)	7.1(-3)	6.8(-3)
4d(^{3}D)*	4.2(-2)	4.0(-2)	3.8(-2)	3.7(-2)	3.5(-2)	3.3(-2)	3.1(-2)	2.9(-2)	2.8(-2)	2.6(-2)
4d(^{3}F)*	8.5(-2)	6.8(-2)	5.9(-2)	5.1(-2)	4.6(-2)	4.1(-2)	3.8(-2)	3.4(-2)	3.1(-2)	2.8(-2)
4s(^{3}S)	3.8(-2)	3.8(-2)	3.7(-2)	3.6(-2)	3.4(-2)	3.3(-2)	3.2(-2)	3.0(-2)	2.9(-2)	2.7(-2)
4p(^{3}P)	5.2(-2)	5.2(-2)	5.1(-2)	4.9(-2)	4.7(-2)	4.5(-2)	4.3(-2)	4.1(-2)	3.9(-2)	3.6(-2)
4d(^{3}D)	4.5(-2)	4.4(-2)	4.2(-2)	4.0(-2)	3.8(-2)	3.6(-2)	3.4(-2)	3.2(-2)	3.0(-2)	2.9(-2)
4d(^{3}F)	8.6(-2)	6.9(-2)	5.9(-2)	5.2(-2)	4.7(-2)	4.2(-2)	3.8(-2)	3.5(-2)	3.2(-2)	2.9(-2)
4s(^{5}S)	6.8(-2)	6.9(-2)	6.7(-2)	6.5(-2)	6.3(-2)	6.1(-2)	5.8(-2)	5.5(-2)	5.3(-2)	5.0(-2)
4p(^{5}P)	8.1(-2)	8.1(-2)	8.0(-2)	7.7(-2)	7.4(-2)	7.1(-2)	6.8(-2)	6.5(-2)	6.1(-2)	5.8(-2)
4d(^{5}D)	7.1(-2)	6.8(-2)	6.5(-2)	6.2(-2)	5.9(-2)	5.6(-2)	5.3(-2)	5.0(-2)	4.7(-2)	4.4(-2)
4d(^{5}F)	1.4(-1)	1.1(-1)	9.8(-2)	8.6(-2)	7.7(-2)	7.0(-2)	6.3(-2)	5.8(-2)	5.3(-2)	4.8(-2)